Elemental Iron: Reduction of Pertechnetate in Presence of Silica and Periodicity of Precipitated Nano-Structures

Journal:	*Environmental Science: Nano*
Manuscript ID	EN-ART-08-2020-000897.R1
Article Type:	Paper

SCHOLARONE™
Manuscripts

Elemental Iron: Reduction of Pertechnetate in the Presence of Silica and Periodicity of Precipitated Nano-structures

Daria Boglaienko[†], Odeta Qafoku[†], Ravi K. Kukkadapu[†], Libor Kovarik[†], Yelena Katsenovich[§], Denis E. Cherkasov[†], Hilary P. Emerson[†], and Tatiana G. Levitskaia[†][*]

[†]Pacific Northwest National Laboratory

[§]Florida International University

[*] Corresponding author: Tatiana.Levitskaia@pnnl.gov

Abstract

Nano-structural transformation of iron minerals in the natural environment is altered and often retarded in the presence of silica (e.g., impeded transformation of ferrihydrite) resulting in a modulated interaction with constituents or contaminants present in groundwater. This phenomenon can significantly affect molecular mechanisms of reduction, precipitation, and sequestration of pertechnetate (TcO_4^-), the most prevalent in the environment chemical form of radioactive contaminant technetium-99, by elemental iron Fe^0 often referred to as zero valent iron (ZVI). Understanding the role of silica in moderating reactivity of Fe^0 toward reduction of TcO_4^- to Tc^{4+} and its interaction with *in situ* formed iron minerals (ferrihydrite, magnetite) is crucial for successful design of a practical separation system and can be related to similar environmental systems. This study was designed to evaluate silica-modified ZVI systems with two commercially available iron materials. The results revealed that the efficiency of TcO_4^- reduction by Fe^0 increased in the presence of silica due to inhibited transformation of iron oxyhydroxide to non-stoichiometric magnetite. Moreover, microscopic evaluation of the newly formed iron mineral phases, both in the presence and absence of silica, revealed unique morphologies related to geological phenomena, such as Orbicular rocks and Liesegang rings, suggesting that iron dissolution/re-precipitation is a rhythmical reaction-diffusion process, which occurs in both micro-scaled and macro-geological environments resulting in layered structures of iron oxidation products.

Environmental significance

Radioactive contaminants pose risks upon their spread in the environment. Studied here pertechnetate is a highly soluble anion of technetium-99, found in the subsurface environments near nuclear wastes storage and reprocessing sites. Application of metallic iron for reductive removal of pertechnetate is a promising method due to its availability, efficiency, low toxicity, and low cost, however, its performance and oxidative transformations are altered in the presence of silica species, common in natural environment. Our results demonstrate enhanced effect of silica on the pertechnetate reduction with *in situ* formed iron minerals. Additionally, evaluation of iron minerals revealed rhythmical formations common in geological structures, relating such phenomena as Orbicular rocks and Liesegang rings to both macro- and micro-scaled systems.

Introduction

The presence of silica in the natural environment affects formation of mineral phases, e.g. transformation of iron minerals in aqueous media. For example, silica-rich groundwaters in Finland and New Zealand contain precipitated ferrihydrite with silica adsorbed to its surface.[1] Ferrihydrite is a poorly crystalline iron oxyhydroxide, which crystallization and transformation into well-ordered iron minerals (e.g., lepidocrocite, goethite, magnetite, and green rust) is stimulated by the electron donor Fe^{2+} and can be hindered by sorbed species, i.e. silica, sustaining ferrihydrite's disordered structure and linking its nano particles into an immobile network.[2-3] In pedogenic environments, it is commonly detected together with lepidocrocite and goethite, however, elevated concentrations of silica impede formation of crystalline lepidocrocite in favor of ferrihydrite.[4] Ferrihydrite has high surface area and reactivity, which makes it an effective sorbent in water treatment.[5-7] For instance, reductive removal of the radioactive contaminant technetium-99 (Tc) predominantly found in subsurface plumes in the form of pertechnetate (TcO_4^-) is a heterogeneous process and requires a solid phase for the efficient exchange of electrons, e.g. *in situ* precipitating ferrihydrite.[8]

Zero-valent iron (ZVI) is a common reductant, effectively used for decontamination of aqueous waste streams from inorganic and organic compounds.[9-13] It has been investigated as a commercially available non-modified material[14-15] and as an engineered material with enhanced efficiency via silica support or cover.[16-21] Supported with silica gel or porous silica ZVI is less prone to agglomeration;[16,22] and covered with silica shell ZVI nanoparticles are characterized by larger surface area, higher mobility, and reduced oxidation.[19] However, the enhanced effect of silica on reduction, sorption, and co-precipitation processes through alteration of iron mineral transformation during Fe^0 oxidation has not been evaluated, and there are no known studies conducted for such systems in the presence of the pertechnetate anion (TcO_4^-).

Technetium-99 (Tc) is a long-lived radionuclide ($2.1\cdot10^5$ years),[23] produced during operation of nuclear reactors and accumulated in the liquid phase of radioactive waste contained in underground tanks of decommissioned complexes, on sites of nuclear fuel reprocessing plants, and in underground plumes. The pertechnetate anion, a dominant form of Tc in systems with oxygen, is highly mobile in subsurface environments and poses a significant risk during radioactive waste processing and disposal. Removal of Tc^{7+} via its reduction to insoluble Tc^{4+} by Fe^0 (ZVI) is one of the treatment options that can be easily implemented due to availability of ZVI materials and their low cost. Our previous studies compared a wide variety of commercially available iron materials[14] and feasibility of ZVI for TcO_4^- reduction at high Tc to Fe loading (1 to 53 mol. ratio) and concomitant fractional incorporation into *in situ* spontaneously formed magnetite.[15] The evidence of Tc-incorporated iron minerals (magnetite, hematite, goethite) was also reported in other studies[24-28], relating this process to the advantages of more environmentally stable forms of mononuclear Tc^{4+} sequestered in the lattice of iron minerals.

Among the previously tested iron products of high purity (97-99.9 %, metal basis) the highest efficiency for reduction of pertechnetate in aqueous solutions was demonstrated by a ZVI material of 75 µm particle size, manufactured by electrolytic method.[14] However, our further investigations revealed that this material was not as efficient as a ZVI containing relatively high levels of impurities, mainly silica. Hence, the objective of this study was to investigate the mechanism of this enhanced reductive removal of TcO_4^- by ZVI in the presence of silica in the relationship to the altered iron mineral transformation. The experimental design of this work is based on evaluation of two commercially available ZVI materials, and is organized as a comparative analysis of series of experiments conducted under different modes of silica addition to ZVI and silica co-precipitation with *in situ* formed iron oxy/hydroxides. The widespread co-existence of silica and iron minerals relates this work to the subsurface environment with natural processes of silica dissolution and precipitation and iron minerals transformation.

Materials and methods

Caution! ^{99}Tc is a β^- emitter with energy 0.29 MeV.[23] The experimental work was conducted at a research nuclear facility by trained personnel.

Materials. Zero valent iron powder 75 µm (200 mesh), denoted in this work as ZVI-A, was obtained from Alfa Aesar. This iron material was manufactured by electrolytic method using steel anodes and ferrous sulfate solution and was of high purity, 99+% (metals basis). Ferox PRB reactive iron powder, 297 µm (50 mesh) was provided by Hepure Technologies Inc. This material, designated as ZVI-B, was produced from cast iron utilizing grinding and pulverizing methods and was composed of 95+% iron, carbon (~ 2.0%), oxygen (< 1%), silicon (1-1.5 %) and trace amounts of phosphorus (< 0.1%) and sulfur (~ 0.1%) according to technical specifications from the manufacturer.

Sodium meta-silicate nonahydrate (crystalline certified from Fisher Scientific, $Na_2SiO_3 \geq 95\%$) was used to prepare amorphous silica gel by dissolution in deionized water followed by direct precipitation with acid. Hydrochloric acid and sodium hydroxide (Fisher Scientific) were used to adjust pH, starting from 12.7 to 5.4. Silica gel was shaken overnight, centrifuged, washed two times with deionized water, and dried in a vacuum oven at 50 °C. The theoretical yield of amorphous silica from 1 g of $Na_2SiO_3 \cdot 9H_2O$ is 0.2420 g of SiO_2. Weight of SiO_2 was monitored daily and drying was stopped as the weight of amorphous silica solids stabilized after 12 days, giving the amount of 0.2795 g. The difference between theoretical and experimental yield is due to the presence of hydration water which is challenging to completely remove.

Solutions were prepared using an NH_4TcO_4 stock (prepared at the Radiochemical Processing Laboratory within Pacific Northwest National Laboratory) and NaCl salt (ACS reagent grade, Fisher Chemical). Deionized water (>18 MΩ·cm) was used to prepare all solutions and reagents.

Study design. The schematic of the experimental design is presented in Figure 1. The small grey boxes on top denote labels of the experimental series (E0 – E6). Amorphous silica prepared by direct precipitation with acid was used without iron material as a control (E0). ZVI-A (99+% Fe^0) was used as received (E1). Another series was composed of the physical mixture of this material with amorphous silica to investigate the effect of the presence of silica not yet reacted with iron (E2). For that purpose, amorphous silica was manually grinded into powder and added to ZVI-A as a mixture of 95 wt.% ZVI-A and 5 wt.% SiO_2. Additionally, this material (ZVI-A) was surface treated via co-precipitation with silica, following the same acid precipitation protocol, described earlier, but in the presence of ZVI-A together with $Na_2SiO_3 \cdot 9H_2O$ in the deionized water (E3); adjustment of pH from the initial value 12.3 to 5.6 was done using 1 M and 0.1 M HCl. In order to see the effect of the acid treatment on iron, a series of ZVI-A without silica, but acid-treated mimicking silica precipitation protocol, was prepared as a control for surface treatment of ZVI-A (E4). Finally, two series of samples using ZVI-B (95+% Fe^0 and 1-1.5 % of Si) as received (E5) and surface treated with acid (E6) as a comparison to the series E4 of the surface treated ZVI-A.

Batch contacts. The samples were prepared in duplicate with 150 mg of ZVI in 40 mL of a solution (phase ratio 0.27 L/g, or concentration 3.75 g/L) containing nominally 0.03 mM TcO_4^- in 0.08 M NaCl, pH 10.50 ± 0.04 (adjusted with 0.1 M NaOH and HCl). Samples were mixed using a shaking table for 20 hours, centrifuged, and decanted filtered to separate supernatant for analysis. The concentration of TcO_4^- was analyzed using liquid scintillation counter (Tri-Carb 2910 TR, PerkinElmer), minimum detectable activity corresponding to $3 \cdot 10^{-8}$ M of Tc, with high sample load scintillation cocktail (Optiphase Hisafe 3, PerkinElmer).

Dissolution kinetics of ZVI-A was studied previously.[14] Kinetics of iron and silicon dissolution for the pristine ZVI-B (150 mg) in 40 mL of 0.08 M NaCl (initial pH 10.50 ± 0.04) together with pH measurements were conducted in triplicate at the time points of 10 min, 20 min, 30 min, 1 hr, 2 hrs, 3 hrs, 5 hrs, 8 hrs and 24 hrs. Control samples (no ZVI; only solution of 0.08 M NaCl, pH 10.50 ± 0.04) were analyzed after reaction for 10 min, 3 hrs, 8 hrs, and 24 hrs. The pH was chosen to achieve a relatively slow oxidation of Fe^0 and, thus, reduction of Tc^{7+}, which would allow comparison of iron materials' reactivities. Samples were centrifuged, and the supernatants (acidified to 0.3 M HNO_3) were analyzed for dissolved iron and silicon with a commercial ICP-OES instrument (Avio 500, PerkinElmer, USA) with the following detection limits for iron and silicon of 0.3 μg/L and 30.2 μg/L, respectively. Data were processed accounting for background iron and silicon (subtraction based on blanks). ICP-OES instrumental parameters: RF power 1300 W, viewing distance 15 mm, integration window 0.02-5 s, sample uptake rate 1.0 mL/min, plasma flow 15 L/min, aux. flow 0.2 L/min, nebulizer flow 0.45 L/min.

All series of batch experiments were conducted at ambient temperature (22 ± 2 °C) and pressure in aerobic environment.

Solid characterization. ***Pre-contact:*** Scanning electron microscopy (SEM, Jeol IT500HR Field Emission Microscope r at 15keV accelerating voltage) was utilized to observe morphological differences in materials in addition to the energy dispersive x-ray spectroscopy (EDX) for chemical composition analysis by an attached detector (Bruker XFlash 6160 with a 60 mm window SDD detector). These analyses were performed on solids prior to contact with aqueous Tc solution.

Post-contact: The Focus Ion Beam/Scanning Electron Microscopy (FIB/SEM) and EDX analyses were performed using an FEI Quanta 3D field emission electron microscope. SEM analysis including point analysis and elemental distribution mapping were collected on thin sections, previously prepared from reacted ZVI samples. Thin sections were prepared by mixing an aliquot of ZVI reacted dry powder (~100 mg) with epoxy resin. The mixture was transferred into a 10 mm base Plexiglas mount, which was degassed and cured overnight under vacuum. The dried mount was cut and polished into 4 mm thin sections. The thin sections were carbon coated with a 10 nm layer by thermal evaporation using a 108C Auto Carbon Coater (Ted Pella, Inc.), which improved sample conductivity, reduced sample charging, and increased the accuracy of SEM/EDX analysis.

Chemical composition data and mapping were collected using an Oxford X-Max 80 mm^2 solid state EDX detector. The EDX analyses were performed using an acceleration voltage of 30 keV and a current of 4 nA. For all the elemental analysis Kα positions were considered. The EDX point analysis were performed using an acquisition time of 60 seconds and elemental mapping were collected with acquisition time of 300 to 600 seconds.

The areas that showed morphological changes and unique patterns were selected and prepared for analysis with Transmission Electron Microscopy (TEM). These areas were extracted from the bulk sample using FIB Ga liquid metal ion source milling and lift-out technique was employed to prepare thin lamellas for TEM analysis. Prior to ion milling, the areas of interest were protected by deposition of 1-2 µm Pt layer using Quanta GIS (gas injection system). The specimens were thinned to □ 80-100 nm by using lower beam currents to below 100 pA.

STEM analysis was carried out with an aberration-corrected JEOL-ARM200F microscope operated at 200 kV. The instrument is equipped with a CEOS GmbH double-hexapole aberration corrector (CESCOR) for the probe-forming lens. The images were acquired with High Angle Annular Dark Field Detector (HAADF) in scanning transmission electron imaging mode. Compositional analysis was performed was performed with a JEOL Centurio high-collection angle silicon drift detector (100 mm^2).

Mössbauer spectra were collected at room temperature for all samples. The 50 mCi ^{57}Co/Rh source and velocity transducer MVT-1000 (WissEL) operated in a mode of constant acceleration (23 Hz, ± 12 mm/s). The signal was transmitted through a holder where radiation was detected by Ar-Kr proportional counter. The counts were stored in a multichannel scalar as a function of energy, utilizing a 1024-channel analyzer. Data were folded to 512 channels to give a flat background and a zero-velocity position corresponding to the center shift (CS or δ) of a metal Fe foil at room temperature. A 25-µm thick Fe foil (Amersham, England) was placed in the same position as the samples to obtain calibration spectra. The Mössbauer data were modeled using the Recoil software (University of Ottawa, Canada) and a Voigt-based structural fitting routine.

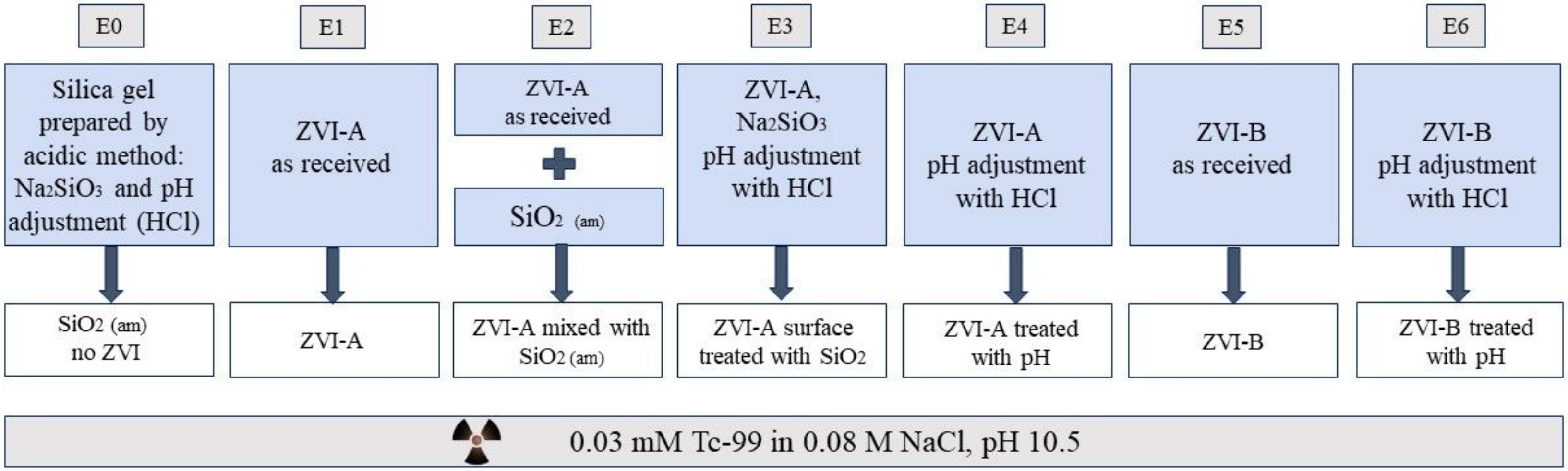

Figure 1. Schematic of the experimental design. ZVI-A is electrolytically manufactured iron (99+% purity, 75 µm; Alfa Aesar); ZVI-B is iron powder produced from cast iron (95+% purity; 297 µm; Hepure Technologies Inc). Grey boxes on top represent labels of the series (E0-E6) used in the figures, and the white boxes represent names of the series referred to in the main text. Large blue boxes contain short descriptions of series, which are fully explained in the study design. The box on the bottom describes the stock solution all the series of experiments were conducted in.

Results and discussion

Characterization of the pre-contact iron materials. Solid characterization of ZVI-A and ZVI-B materials via scanning electron microscopy (SEM) before the contact with aqueous media can be found in SI (Figure SI-1); and via dispersive x-ray analysis (EDX), which provides visual evidence of silica particles among the particles of iron in ZVI-B as received (Figure SI-2). Room temperature comparative Mössbauer analysis between ZVI-A and ZVI-B (Figure SI-3) supported the evidence of additional sites in ZVI-B, which were previously studied as structural silicon in the Fe-Si alloy.[29] Thus, both structural silicon and particulate silica was identified in ZVI-B material.

The dissolution kinetics of ZVI-A were studied before[14] and revealed the highest initial (within 10 min sampling time) concentrations of dissolved Fe^{2+}, which declined rapidly with time. The dissolution kinetics for the ZVI-B (Figure 2) showed similar behavior so that concentration of dissolved Fe increased significantly within first 20 min, followed by a sharp decrease up to one hour with possible formation of precipitating iron oxyhydroxides, and reaching a steady-state for Fe^{2+} dissolution (eq. 1) and precipitation (eq. 2). The changes in pH (Figure 2) with the overall decrease to 9.93 ± 0.09 towards the time period of 24 hours are indicative of the dominant processes of iron oxyhydroxides and oxides formation and precipitation during that time. Differences between concentrations of dissolved iron from ZVI-A as received (up to 12 μM after 3 hours for initial concentration 0.5 g/L)[14] and ZVI-B as received (predominantly below 35 μM after 3 hours for initial concentration 3.75 g/L) can be related to the effect of the silica/silicon presence in ZVI-B.

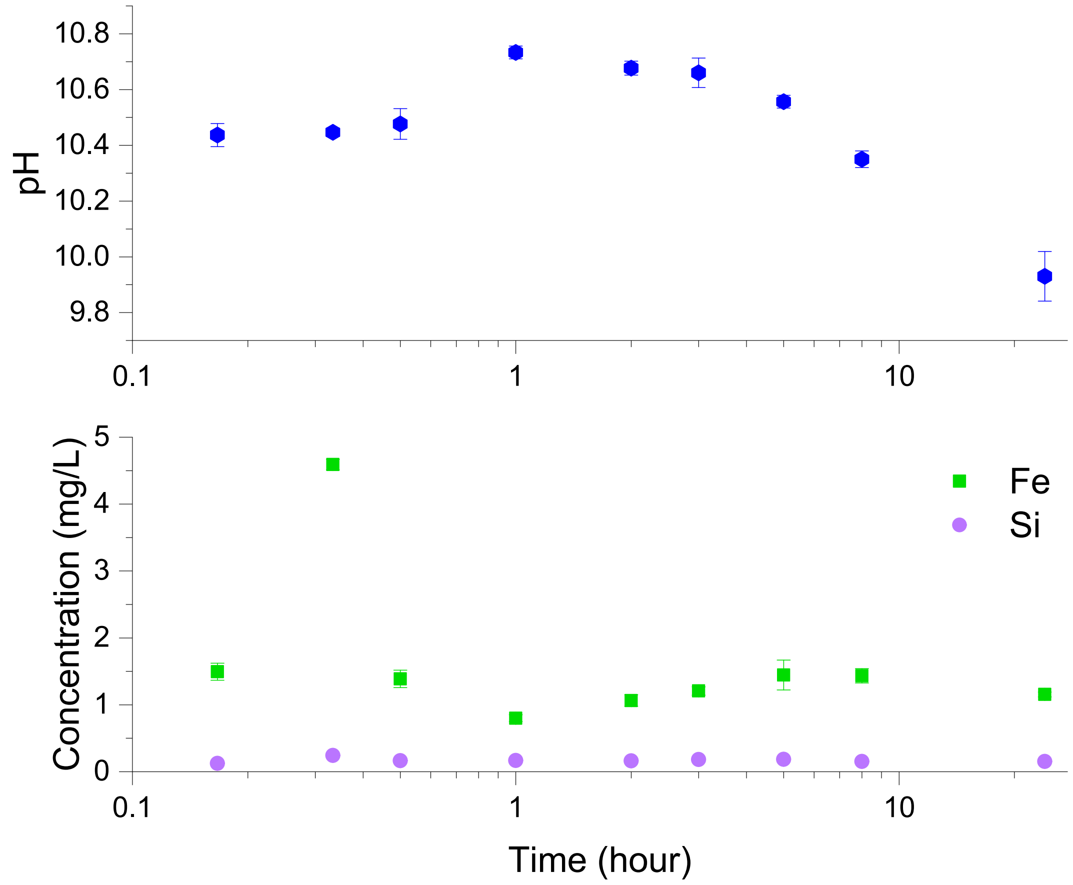

Figure 2. Iron and silicon dissolution using ZVI-B (as received) in 0.08 M NaCl and pH measurements upon dissolution of this material.

The general process of metallic iron dissolution in the presence of silica can be presented as follows. Oxidation of Fe^0 by water under aerated conditions[30]:

$$2Fe^0 + O_2 + 2H_2O \rightarrow 2Fe^{2+} + 4OH^- \qquad (1)$$

where Fe^{2+} dissolved species are predominantly $Fe(OH)^+$ and aqueous $Fe(OH)_2$.

Further oxidation of Fe^{2+} in the presence of oxygen can be written as:

$$2Fe(OH)_{2(aq)} + O_2 \rightarrow 2FeOOH + 2OH^- \qquad (2)$$

Reactions described by the eq. (1) and (2) imply that at high pH (i.e., 10.5 ± 0.04) oxidation of Fe^0 to Fe^{2+}, and Fe^{2+} to Fe^{3+} does not proceed as rapidly as for low pH range, and the choice of this pH was dictated by the necessity to achieve the slower kinetics of the Tc^{7+} reduction, at which differences in reductive behavior of different iron materials are traceable and comparable.

The effect of 0.08 M NaCl, which composes the solution matrix, is not considered to be significant here, as the $FeCl^+$ concentrations decline far below 1 μM at pH > 9 (Geochemist's workbench version 12.0 modelling for a similar system with metallic iron dissolved in 0.08 M NaCl).[14]

Iron oxyhydroxide, which can include goethite (α-FeOOH), lepidocrocite (γ-FeOOH), or ferrihydrite (several chemical formulas exist, $5Fe_2O_3{\cdot}9H_2O$, $Fe_5HO_8{\cdot}4H_2O$, or $FeOOH{\cdot}0.4H_2O$),[31] is an intermediate product in alkaline solutions, where magnetite (Fe_3O_4) forms via adsorption of Fe^{2+} on FeOOH, eq. (3), and via transformation of iron oxyhydroxide, eq. (4), as it was investigated for γ-FeOOH in alkaline conditions by Tamaura et al.[32]:

$$2FeOOH + \ Fe^{2+} + H_2O \rightarrow [FeOOH]_2FeOH^+ + H^+ \tag{3}$$

$$[FeOOH]_2FeOH^+ \rightarrow Fe_3O_4 + H_2O + H^+ \tag{4}$$

As discussed in the following subsection, magnetite, along with Fe^{3+} oxyhydroxide, was formed in all series, ZVI-A and ZVI-B, with and without silica (E1-E6).

The effect of silica on iron transformation is known in literature[31,33,34] and is expected to impact TcO_4^- reduction by metallic iron. Thus, experimental series E2 and E3 were designed to amend ZVI-A (99+% pure Fe^0) with silica as a physical mixture (E2) and surface treated iron (E3) and compare its reductive efficiency to ZVI-B. Silica gel was synthesized according to eq. (5):

$$Na_2SiO_3 + H_2O + 2HCl \rightarrow Si(OH)_4 + 2NaCl \tag{5}$$

and added to ZVI-A in order to evaluate the efficiency of iron-silica mixture upon dissolution of both Fe^0 and SiO_2 (series E2). In series E3, iron oxides/oxyhydroxides were formed in the presence of silicic acid in the solution, i.e. co-precipitated with silica. Iron (ZVI-A) particles were contacted with sodium metasilicate solution (pH > 12) and treated with HCl to obtain silicic acid, which produces silica hydro gel (SiO_2) during further polymerization and loss of water.[35] Series E5 and E6 had structural silicon and silica impurities in the iron material (ZVI-B).

The dissolution kinetics of particulate silica and silicon incorporated into the ZVI-B material during its manufacturing reveals steadily low concentrations of silicon in the supernatant (Figure 2a) amounting to less than 0.5 % of the total Si in the system, which is estimated to be approximately 35.7 mg/L in 3.75 g/L ZVI-B, if more conservative number of 1 wt.% Si impurities is considered according to the manufacturer specification. Undissolved Si particles are visible on the EDX map obtained after contact of ZVI-B with 0.03 mM TcO_4^- in 0.08 M NaCl solution (Figure SI-4).

The amount of dissolved Si is significantly less than reported previously in a range from 100 to 150 mg/L over a wide pH range at room temperature in the absence of iron.[36] Low dissolution rates of silicon can be explained by complexation of silicic acid and dissolved Fe^{2+} species, as well as sorption to the surface of iron hydroxides and oxyhydroxides. The existence of monomeric and dimeric silica surface complexes on iron sites has been examined in previous studies.[35,37,38] Monomeric species $FeSiO_2(OH)_2^+$ and $FeSiO(OH)_3^{2+}$ are formed during contact of iron hydroxides and silicic acid; whereas soluble dimeric silica can be formed according to the reaction[37] with liberation of H^+ ions:

$$2Si(OH)_4 \rightarrow Si_2O_2(OH)_5^- + H^+ + H_2O \tag{6}$$

As a result, iron hydroxide and oxyhydroxide surface is covered with the dimeric species $FeSi_2O_3(OH)_4^{+}$ and $FeSi_2O_2(OH)_5^{2+}$ with high sorption densities, previously observed at silica concentrations below 50 mg/L and pH 7.25 and 9.5.[37] Moreover, another study showed that higher pH leads to stronger adsorption of silica on ferrihydrite[38] since pKa_1 values of monomeric silicic acid is 9.8 and oligomeric silicic acid is in the range of 9.5-10.7 at room temperature.[39] It also revealed that, besides monodentate-mononuclear complexes of silica monomers formed at loadings up to 0.5 mM, silicate oligomers, or polymers, covered the surface as bidentate-binuclear complexes (Si – O – Si bonds) at concentrations of 1-2 mM Si. This result is supported by other studies demonstrating polymerization of silica on the ferrihydrite surface at concentration of 1 mM and pH range 7-9,[40] and detection of oligomeric silica species on magnetite and maghemite at the concentrations of 0.4-5 mM and alkaline pH.[41] Here, at the conditions of alkaline pH and Si concentrations of approximately 1.4 mM in ZVI-B (E5 and E6), 2.3 mM in ZVI-A co-precipitated with sodium metasilicate (E3), and 3.2 mM Si in the mixture of ZVI-A and silica gel (E2), silica oligomers, or polymers, are expected to bind to the surfaces of iron oxides and oxyhydroxides formed in these series.

Reduction of TcO_4^-. Oxidation of Fe^{2+} to Fe^{3+} allows reduction of Tc^{7+} to Tc^{4+} and proceeds accordingly:

$$TcO_4^- + 3Fe^{2+} + (n+7)H_2O \rightarrow TcO_2 \cdot nH_2O(s) + 3Fe(OH)_{3(s)} + 5H^+ \qquad (7)$$

where aqueous Fe^{2+} is the electron donor.[8]

Results obtained within the time period of 20 hours showed complete reduction of TcO_4^- in all systems, except the control composed of silica without ZVI (Figure 3, series E0). The differences in reduction can be discerned for the 3-hour period of time, where the aqueous non-reduced fraction of TcO_4^- was below 0.3 in all the series of metallic iron containing silica/silicon, i.e., ZVI-A amended with silica (series E2 and E3), and ZVI-B (series E5 and E6) which initially had particulate silica and structural silicon. The series with ZVI-A as received (E1) showed the lowest TcO_4^- removal efficiency (Figure 3).

Treatment of iron (ZVI-A) with sodium silicate and acid did not enhance its performance in comparison to ZVI-B as received and ZVI-B treated in the same manner with acid (E3 vs E5 and E6). However, the presence of sodium silicate enhanced iron reactivity as compared to the sample without silica but similarly treated with HCl to reduce pH (E3 vs E4). Overall, acid treatment slightly improved reduction efficiency, as evident from ZVI-A treated (E4) and ZVI-A non-treated (E1); acid treated samples of ZVI-B (E6) showed almost complete reductive removal of Tc from the aqueous fraction, as well as non-treated samples of ZVI-B (E5). Addition of amorphous silica to the ZVI-A samples (E2, no acid treatment) resulted in the most drastic improvement of the Tc reduction compared to ZVI-A material as received. This series, E2, was intended to simulate ZVI-B series of samples, E5, and succeeded in the goal of TcO_4^- reduction efficiency improvement, hence, revealing the role of silica in the ZVI-B material, where the presence of silica "impurities" should be considered as an "enhancing agent".

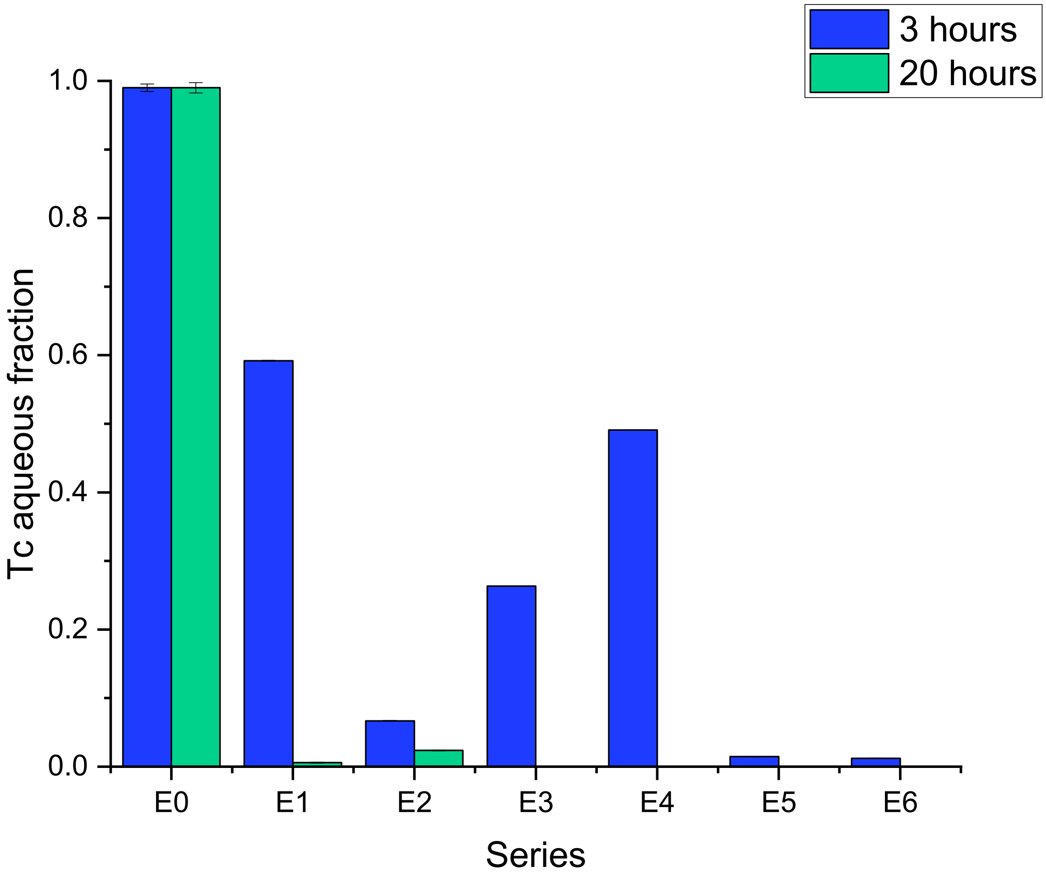

Figure 3. Reduction of Tc^{7+} (TcO_4^-) in six series (E1-E6) of two ZVI materials (ZVI-A and ZVI-B), pristine and modified with silica and acid treatment (see Figure 1); E0 is the control series with amorphous silica and no ZVI.

Characterization of the post-contact solid phase. Mössbauer analysis was carried out on all the series with ZVI-A and ZVI-B to compare formation of different iron minerals after a 20-hour reaction time of iron materials with TcO_4^-. According to Figure 4, all samples are dominated by Fe^0 sextets, implying on a significant amount of unreacted ZVI in a sample.

Two overlapping minor sextets of octahedral-tetrahedral Fe^{3+} and octahedral $Fe^{2.5+}$, which belong to non-stoichiometric magnetite, and/or magnetite and maghemite mixture, are present in all series as well. Magnetite, which is composed of both Fe^{3+} and Fe^{2+} atoms, would oxidize to maghemite in an aerobic environment.[42] The Fe^{2+}/Fe^{3+} ratio[43] serves as evidence of magnetite partial oxidation, ranging from 0.5 for pure magnetite to 0 for pure maghemite. The ratio estimates are given for each sample in Figure 4 and are indicative of partially oxidized magnetite in all series. Even though magnetite and maghemite mixture can also be characterized by the Fe^{2+}/Fe^{3+} ratio < 0.5, it is impossible to differentiate magnetite and maghemite mixture from the partially oxidized (non-stoichiometric) magnetite via Mössbauer analysis.

Further, a doublet of Fe^{3+} with quadrupole splitting of, averaged for six samples, □0.5 mm/s is distinguished in all the collected spectra. It can be a composite of multiple phases including ferrihydrite, lepidocrocite, and nano-sized goethite, magnetite or maghemite.[8,44-47] Considering initial conditions of pH 10.5 ± 0.04, ambient atmosphere, 0.08 M NaCl, and relatively short reaction time (20 hours), the iron transformation pathway would likely be directed towards ferrihydrite formation with further transformation to magnetite during adsorption of Fe^{2+} at alkaline solutions, eq. (3)-(4),[32] and to goethite and lepidocrocite during dissolution-precipitation and crystallization of ferrihydrite or iron hydroxide. However, lepidocrocite formation is known to be suppressed in the presence of silica, but the ferrihydrite and goethite couple is often found in natural environments with relatively high Si content in water, e.g., bog iron ores, lake ores, and placic horizons.[1] Green rust is another theoretically possible product of ferrihydrite transformation, but it forms at weakly acidic or weakly alkaline solutions, and microscopy analysis (absence of hexagonal plates) and Mossbauer data (no evidence of Fe^{2+} signal) do not support its presence in these samples.

There are known effects of common in natural environment impurities, Si and Al, on iron mineral transformation, however the mechanisms are different.[2,4,31,33,48] Aluminum impedes transformation of ferrihydrite by decreasing Fe^{2+} retention on ferrihydrite[48]. Binding of silica monomers or oligomers to the ferrihydrite crystal growth sites inhibits its further transformation by blocking crystal growth sites and stabilizing disordered structure.[2,31,33] However, the inhibition depends on the molar ratio of Si to Fe, and transformation of ferrihydrite still proceeds at the ratio of approximately 3 %, with almost complete inhibition at the ratio 5.8 % and higher.[2] In the present study, at the ratios of 2-4.7 %, transformation of ferrihydrite is slowed but not fully suppressed.

It is important to note that a clear Mössbauer signal related to Fe^0 with structural silicon is identified in the ZVI-B samples (E5 and E6), Figure 4. This signal is supported via analysis of the pristine ZVI-B materials (Figure S3a), where signals from the Fe environment containing from 1 to 3 Si atoms are identified. Such Fe-Si alloys were studied in detail by Overmann et al.[29], whose results, in relation to our ZVI-B material, suggest approximately 5 wt.% of silicon in iron.

All the silica containing samples (E2, E3, E5, and E6) exhibited more efficient TcO_4^- reduction (Figure 3), and most of them are characterized by the larger amount of Fe^{3+} mineral content than no-silica containing samples (predominantly, ferrihydrite, as discussed in the following section). This can be related to the effect of high surface area of ferrihydrite (> 200 m^2/g;[31] or 200-800 m^2/g[6]), and, more importantly, to higher concentrations of sorbed Fe^{2+}, which can be more than three times that observed for ferrihydrite compared to that on goethite with similar surface area.[49] It can also be explained by the retardation effect of silica on ferrihydrite transformation, i.e. complexation on the surface of ferrihydrite and with dissolved Fe^{2+}, discussed earlier, that impedes its crystallization. Thus, ferrihydrite serves as the amorphous media with highly developed surface for more efficient heterogeneous Tc reduction, i.e., the $Fe^0 – Tc^{7+}$ redox process that occurs not as extensively and rapidly in aqueous phase as on the surface of the *in situ* formed iron minerals.[8]

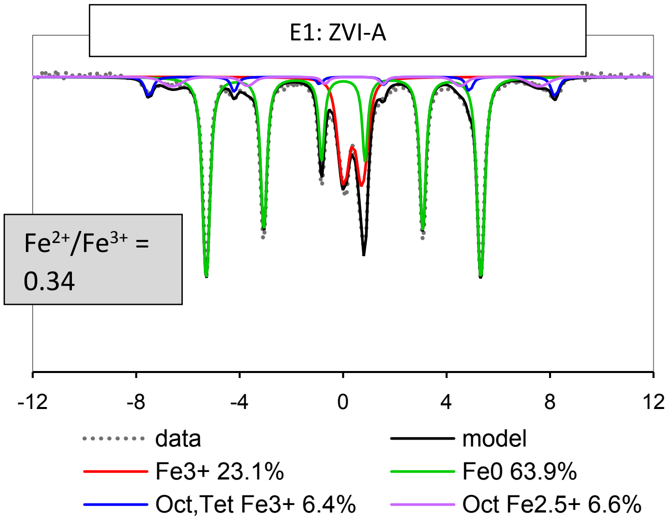
E1: ZVI-A
Fe2+/Fe3+ = 0.34
-12
-8
-4
0
4
8
12
data
model
Fe3+ 23.1%
Fe0 63.9%
Oct,Tet Fe3+ 6.4%
Oct Fe2.5+ 6.6%

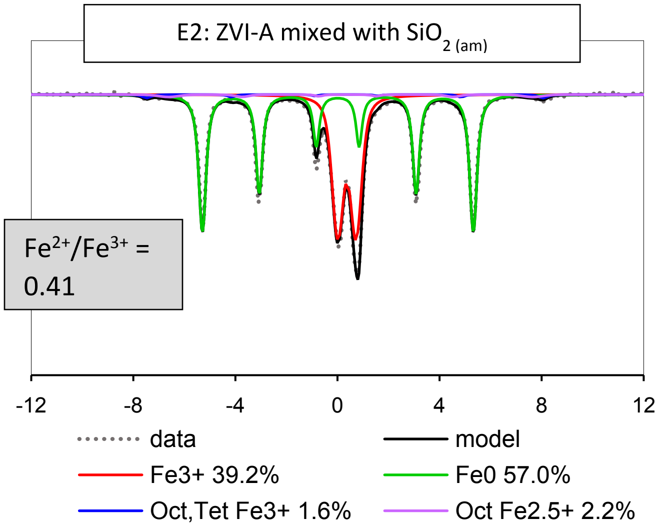
E2: ZVI-A mixed with SiO2 (am)
Fe2+/Fe3+ = 0.41
-12
-8
-4
0
4
8
12
data
model
Fe3+ 39.2%
Fe0 57.0%
Oct,Tet Fe3+ 1.6%
Oct Fe2.5+ 2.2%

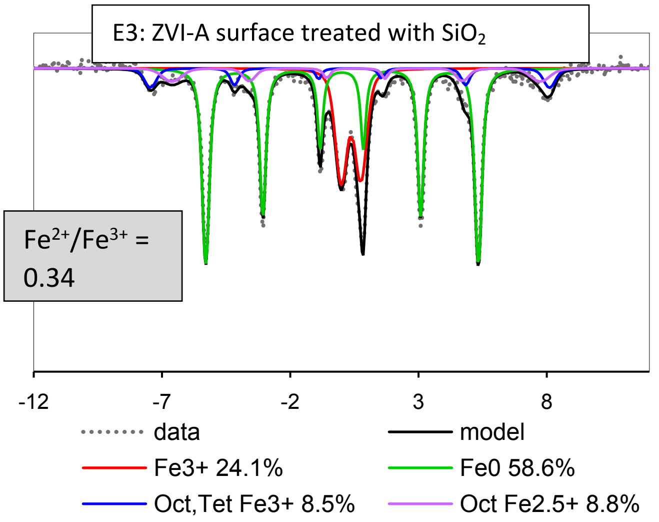
E3: ZVI-A surface treated with SiO2
Fe2+/Fe3+ = 0.34
-12
-7
-2
3
8
data
model
Fe3+ 24.1%
Fe0 58.6%
Oct,Tet Fe3+ 8.5%
Oct Fe2.5+ 8.8%

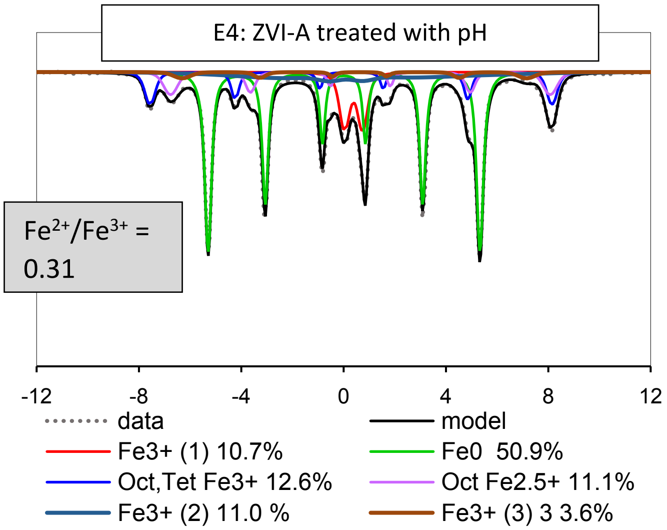
E4: ZVI-A treated with pH
Fe2+/Fe3+ = 0.31
-12
-8
-4
0
4
8
12
data
model
Fe3+ (1) 10.7%
Fe0 50.9%
Oct,Tet Fe3+ 12.6%
Oct Fe2.5+ 11.1%
Fe3+ (2) 11.0 %
Fe3+ (3) 3 3.6%

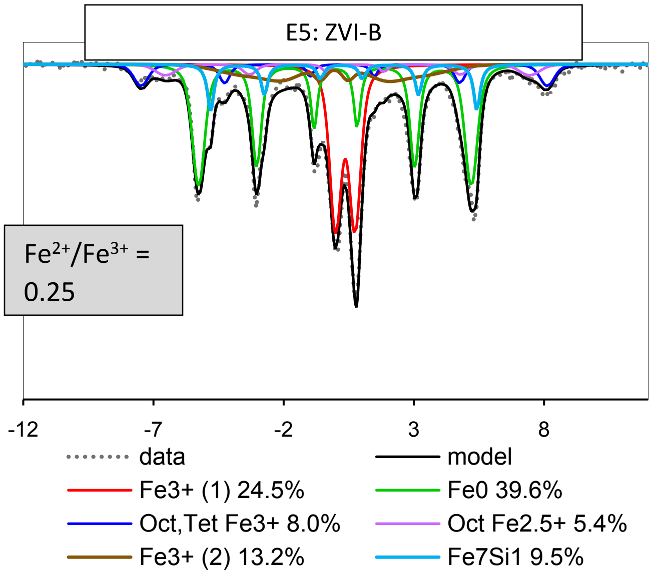
E5: ZVI-B
Fe2+/Fe3+ = 0.25
-12
-7
-2
3
8
data
model
Fe3+ (1) 24.5%
Fe0 39.6%
Oct,Tet Fe3+ 8.0%
Oct Fe2.5+ 5.4%
Fe3+ (2) 13.2%
Fe7Si1 9.5%

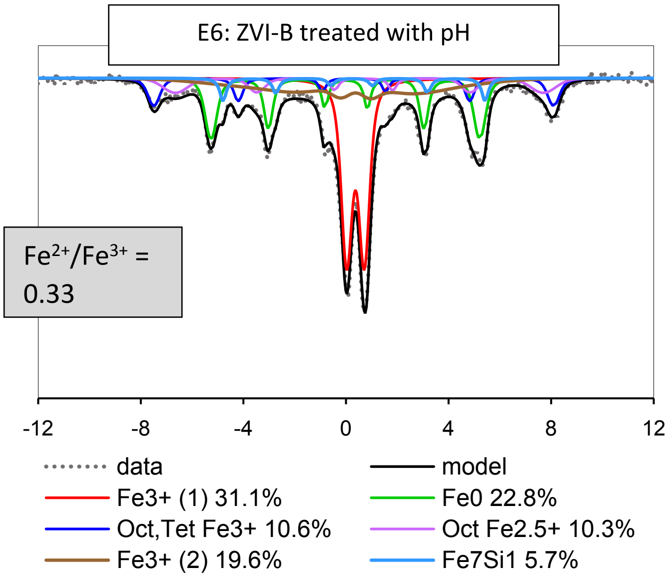
E6: ZVI-B treated with pH
Fe2+/Fe3+ = 0.33
-12
-8
-4
0
4
8
12
data
model
Fe3+ (1) 31.1%
Fe0 22.8%
Oct,Tet Fe3+ 10.6%
Oct Fe2.5+ 10.3%
Fe3+ (2) 19.6%
Fe7Si1 5.7%

Figure 4. Room temperature Mössbauer spectra for six series (E1-6) of two ZVI materials (ZVI-A and ZVI-B) and Fe^{2+}/Fe^{3+} ratio as an evidence of partial oxidation of magnetite (< 0.5).

Microscopic evidence of the unique morphology. Scanning electron and transmission electron microscopies (SEM and TEM) together with energy dispersive x-ray analysis (EDX) were employed to reveal morphologic nature of the post-contact samples of series E1-E6 (Figure 5; Figure SI-5a). Surprisingly, orbicular formations with layered or concentric structures can be discerned in all the series, especially in the series E1, E2, and E5, which were not pre-treated with low pH solutions, hence, iron oxidation steps differed. The layered structure was also observed in the series not yet exposed to Tc solution (Figure SI-5b).

Close-up micrographs of each post-contact series are represented by the right image in the triads, where rather amorphous and round formations suggest iron hydroxide and ferrihydrite in all the series, and needle-like crystals suggestive of goethite are noticeable in series E4 (acid treated ZVI-A without silica). The layered structure of oxidized iron is clearly seen in the right image of the series E1 (ZVI-A), and EDX analysis was carried out aiming to the compare composition of each of the layers (Table SI-1, Figure SI-6). As presented in Table SI-1, iron content in the locations 2, 4, and 6 is slightly higher than in the locations 1, 3, 5, and 7. This provides evidence of different densities of iron oxide or oxyhydroxide in layers, or periodicity in layering of different species of iron hydrolysis. Liesegang ring patterns formed during iron oxide growth on carbon steel coupons were also reported by Do et al.,[50] coupling this phenomenon to Ostwald ripening of oxides (supersaturation theory), which is one of the theoretical approaches among others including adsorption, sol coagulation, diffusion wave, and phase separation theories[51,52]. More studies are warranted to investigate this process.

TEM and EDX analyses were conducted on the series E5 sample (ZVI-B). The area selected for FIB extraction is shown on the center image in E5 triad (Figure 5). The lamella presents the layered structure previously observed with SEM. TEM analysis revealed that the layered structure was composed of metallic iron (Figure 6a) along with 2-line ferrihydrite as a matrix embedding possibly goethite and/or lepidocrocite "wavy" structures, identified via selected area electron diffraction (SAED) patterns (Figure 6b). EDX maps show concentrated silica along the edges of metallic iron, which might imply on the bonding of silica polymers with the newly formed products of iron oxidation on the surface of the metal. Environmental levels of TcO_4^- used in this study (0.03 mM) did not allow for Tc identification via EDX analysis.

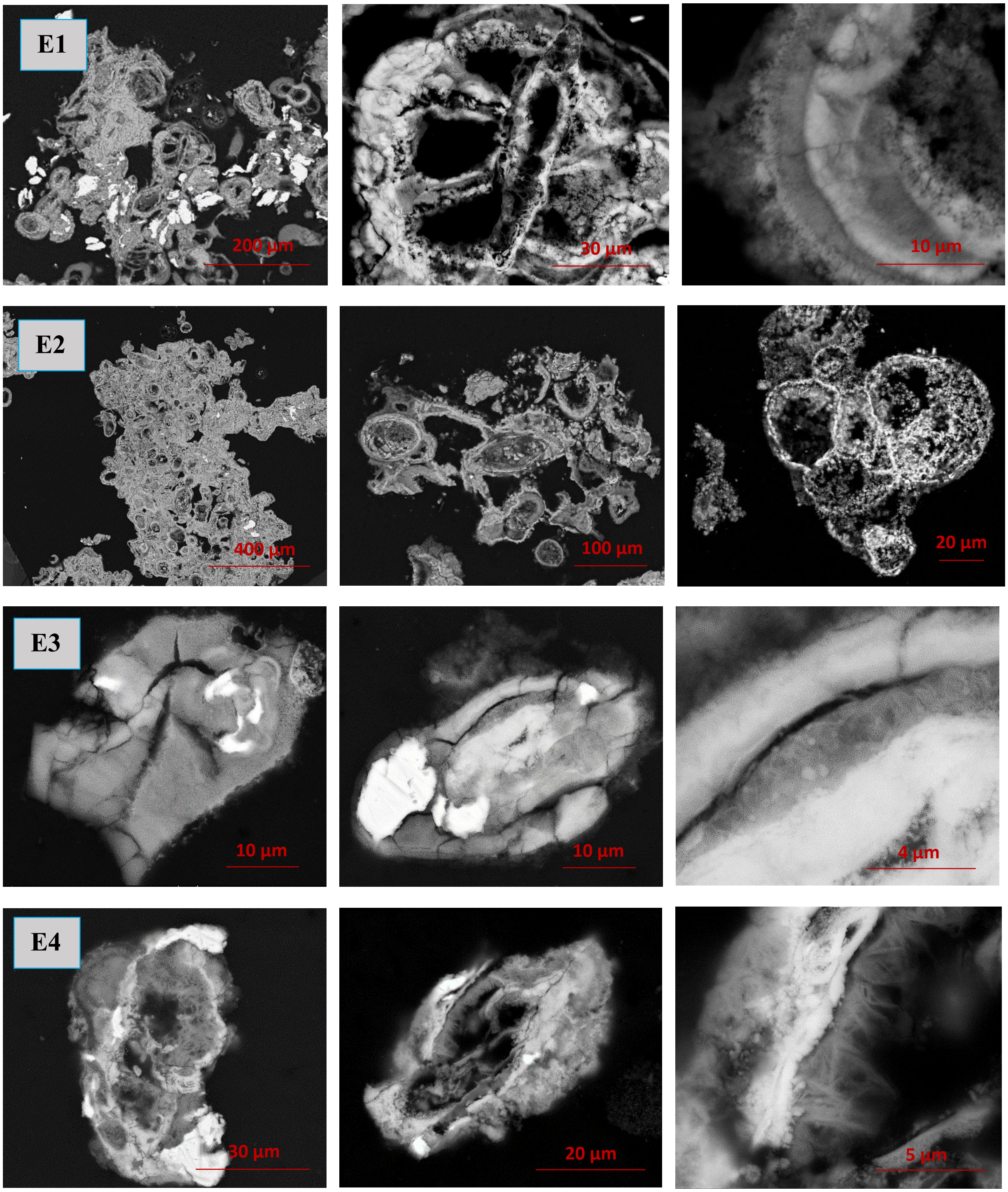
E1
200 µm
30 µm
10 µm
E2
400 µm
100 µm
20 µm
E3
10 µm
10 µm
4 µm
E4
30 µm
20 µm
5 µm

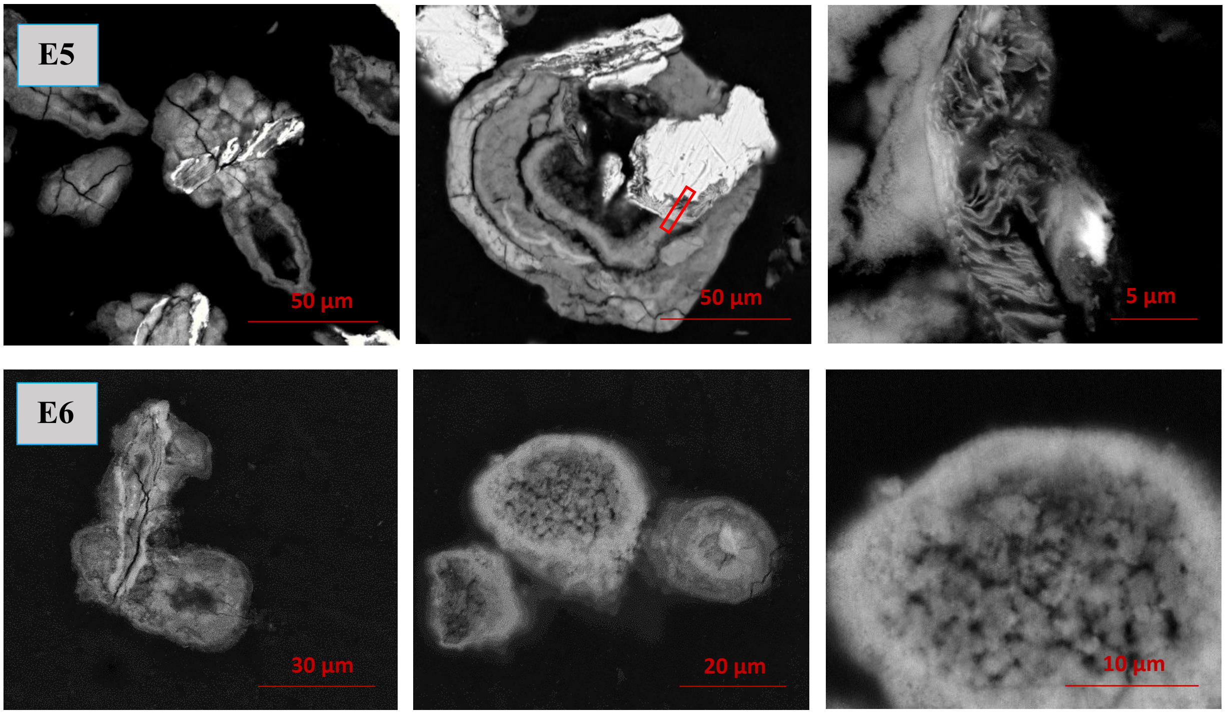

Figure 5. SEM images of the experimental series (E1-E6) after contact with 0.03 mM TcO_4^- in 0.08 M NaCl solution. Red shape on the central image in series E5 shows the area selected for FIB extraction.

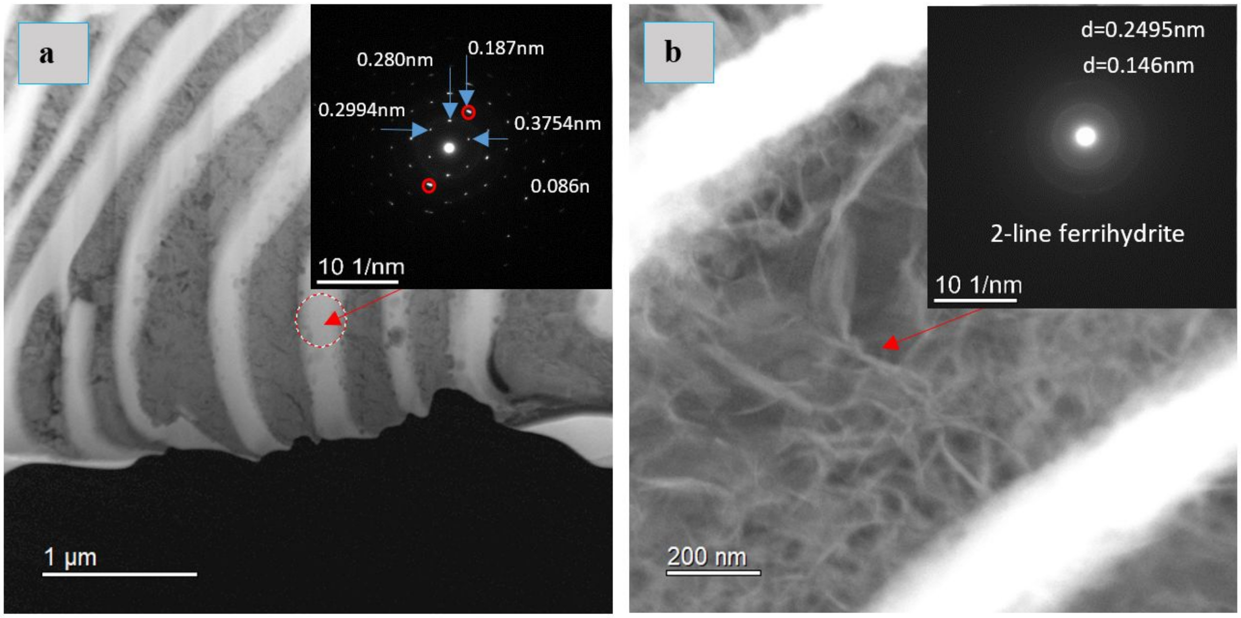

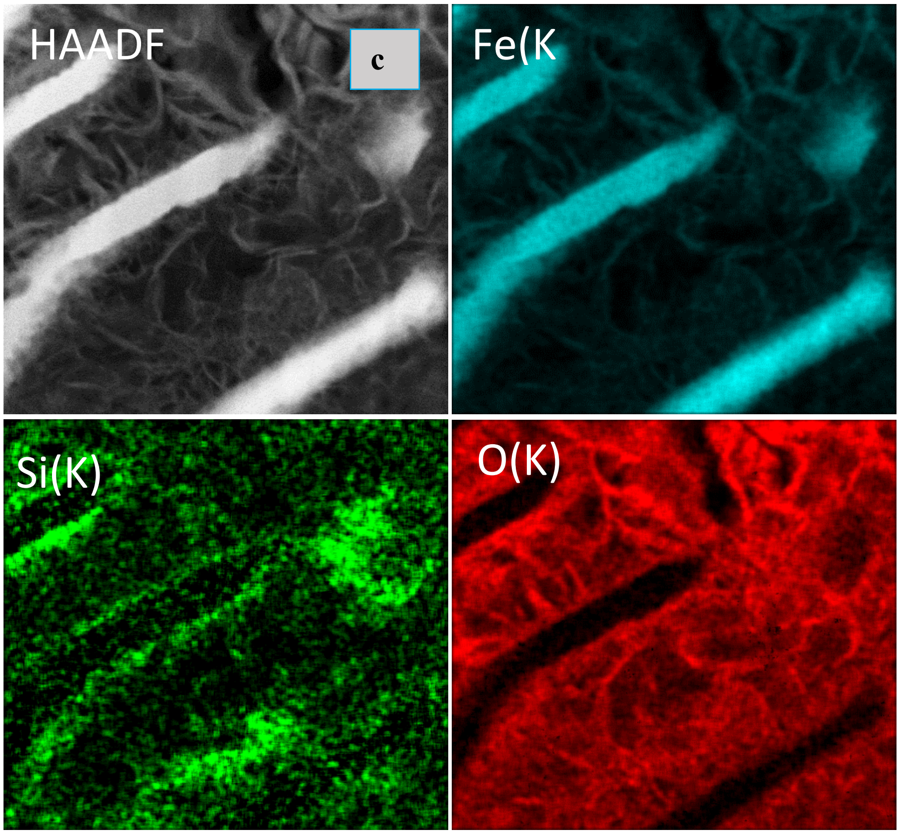

Figure 6. TEM images and EDX analyses of the FIB extraction of the E5 sample (FIB area is shown in Figure 6 on the central image belonging to E5). (a) Selected area electron diffraction (SAED) pattern showing iron BCC structure, and (b) ferrihydrite with lepidocrocite or goethite. (c) TEM image of a sample and EDX maps of Fe, Si, and O.

Relation to geological phenomena. The layered morphology of iron oxyhydroxides, discovered via SEM analysis, is analogous to such phenomena known in geology as orbicular rocks and Liesegang rings. Orbicular rocks are formed due to rhythmical layering, resulting in concentric shells of different texture and composition, and are common throughout the world without relation to a specific geologic setting or chemical environment.[53] They are often compared to Liesegang rings, which are formed in gelatinous or porous substrates of reaction-diffusion systems. There is no single theory agreed upon to explain the process governing all the variety of such phenomena;[51,54] however, an explanation given in the review by L'Heureux proposes interaction between the processes of diffusion of dissolved species and kinetics of formed precipitates.[55]

The mathematical model developed by H. Meinhardt[56] successfully replicates the elementary steps of the process of biological pattern formation, and is based on the autocatalytic activator-inhibitor or, in our case, activator-substrate interactions, expressed as:

$$\frac{\partial a}{\partial t} = sba^{*2} - r_a a + D_a \frac{\partial^2 a}{\partial x^2} \tag{9}$$

$$a^{*2} = \frac{a^2}{1 + s_a a^2} + b_a \tag{10}$$

$$\frac{\partial b}{\partial t} = b_b(x) - r_b b + D_b \frac{\partial^2 b}{\partial x^2} \tag{11}$$

where *a(x)* is the activator (oxidized iron, i.e. iron hydroxide), *b(x)* is the substrate (release of Fe^{2+}), t is time, D_a and D_b are the diffusion coefficients ($D_a >> D_b$), r_a and r_b are the decay (removal) rates, and s is the rate constant of the autocatalytic term.[56]

Formation of a layer of iron hydroxide/oxyhydroxide leads to depletion of dissolved iron and inhibition of the layer growth, which reoccurs once there is enough substrate. i.e. time-dependent supply of the dissolved iron. The code based on this model[56] simulates rich variety of patterns, found in nature, throughout different display modes and controllable parameters from the eq. (9)-(11). Figure 7 presents the modelled pattern and its comparison to the dominant morphologies observed in this study. Overall, our study reveals the phenomena of periodicity and rhythmical layering observed at micro/nano scale during iron dissolution and re-precipitation, similar to the geological structures occurring at macro scale (Orbicular rocks and Liesegang rings).

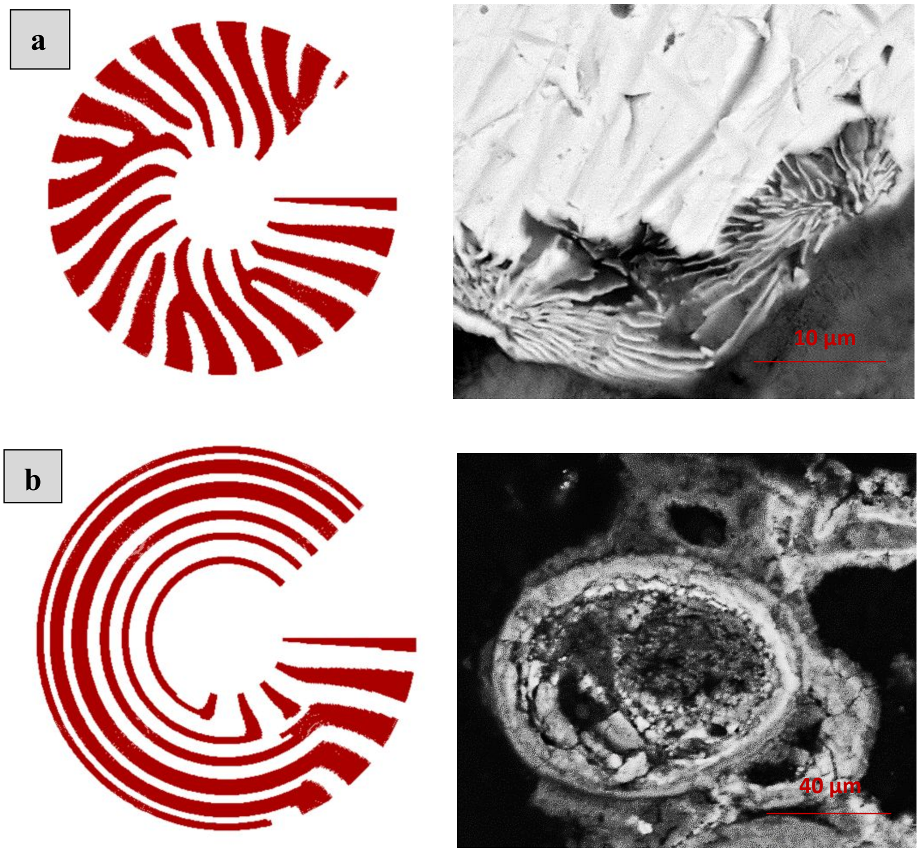

Figure 7. Iron hydroxide rings simulated and observed. (a) simulation of the layered structure observed in the sample E5; (b) simulation of concentric or orbicular structure observed in the

sample E2. Changes in the simulation model are due to different diffusion coefficients, (a): D_a = 0.06 and D_b = 0.15; (b): D_a = 0.002 and D_b = 0.35, adjusted empirically.

Conclusions

Oxidation of the metallic iron and concurrent *in situ* transformation of iron oxides and oxyhydroxides are complex processes that can be altered by the presence of other dissolved or incorporated species, i.e. silica monomers or polymers. The mechanisms of these processes have relevance to both natural environment, where concomitant dissolution of iron minerals and silica is common in aqueous systems, i.e. groundwater, and anthropogenically impacted environment with introduced contaminants, i.e. highly mobile in subsurface TcO_4^-. As shown in this study, the effect of silica on TcO_4^- reduction is indirect, via impeded transformation of iron oxyhydroxides (mainly ferrihydrite) into non-stoichiometric magnetite, which in turn provides highly developed surface of ferrihydrite for heterogeneous reduction of TcO_4^-. Here, heterogeneity implies that redox reaction occurs on the surface of a solid phase, and the co-existence of both dissolved iron (reductant) and pertechnetate (oxidant) in aqueous phase is not sufficient for the effective process of the electron exchange. Furthermore, the complexity of iron dissolution and re-precipitation manifests itself through the rhythmical layering that is initiated and observable on a micro/nano scale and is related to the natural phenomena of Orbicular rocks and Liesegang rings commonly found among geological structures.

Conflicts of interests

There are no conflicts to declare.

Acknowledgements

It is our pleasure to acknowledge help of T. H. Beasley (FIU FCAEM) and PNNL researchers C. T. Resch, N. L. D'Annunzio, S. Chatterjee, G. B. Hall, and C. H. Delegard. This research was supported by the U.S. Department of Energy's Office of Environmental Management and performed as part of the Technetium Management Hanford Site project at the Pacific Northwest National Laboratory (PNNL) operated by Battelle for the U.S. Department of Energy under Contract No. DE-AC05-76RL01830. This work was in part supported by the Department of Energy Minority Serving Institution Partnership Program (MSIPP) managed by the Savannah River National Laboratory under SRNS contract DE-AC09-08SR22470. Part of this research was performed at EMSL, a national scientific user facility at PNNL managed by the Department of Energy's Office of Biological and Environmental Research. Postdoctoral appointment of DB at PNNL is gratefully acknowledged.

References

1. U. Schwertmann, The effect of pedogenic environments on iron oxide minerals, *Advances in Soil Science*, Springer, New York, NY, 1985, **1**, 171-200.

2. X. Wang, M. Zhu, S. Lan, M. Ginder-Vogel, F. Liu and X. Feng, Formation and secondary mineralization of ferrihydrite in the presence of silicate and Mn(II), *Chem. Geol.,* 2015, **415**, 37-46.

3. R. M. Cornell, R. Giovanoli and P. W. Schindler, Effect of silicate species on the transformation of ferrihydrite into goethite and hematite in alkaline media, *Clay Clay Miner.,* 1987, **35**, 21-28.

4. U. Schwertmann, Occurrence and formation of iron oxides in various pedoenvironments. In: J. W. Stucki, B. A. Goodman and U. Schwertmann (eds), Iron in Soils and Clay Minerals, NATO ASI Series (Series C: Mathematical and Physical Sciences), **217**, Springer, Dordrecht, 1988.

5. G. A. Waychunas, B. A. Rea, C. C. Fuller and J. A. Davis, Surface chemistry of ferrihydrite: Part 1. EXAFS studies of the geometry of coprecipitated and adsorbed arsenate, *Geochim. Cosmochim. Acta,* 1993, **57**, 2251-2269.

6. A. C. Scheinost, S. Abend, K. I. Pandya and D. L. Sparks, Kinetic controls on Cu and Pb sorption by ferrihydrite, *Environ. Sci. Technol.,* 2001**, 35**, 1090-1096.

7. L. Tian, Z. Shi, Y. Lu, A. C. Dohnalkova, Z. Lin and Z. Dang, Kinetics of cation and oxyanion adsorption and desorption on ferrihydrite: Roles of ferrihydrite binding sites and a unified model, *Environ. Sci. Technol.,* 2017**, 51**, 10605-10614.

8. J. M. Zachara, S. M. Heald, B.-H. Jeon, R. K. Kukkadapu, C. Liu, J. P. McKinley, A. C. Dohnalkova and D. A. Moore, Reduction of pertechnetate [Tc(VII)] by aqueous Fe(II) and the nature of solid phase redox products, *Geochim. Cosmochim. Acta,* 2007, **71**, 2137-2157.

9. Y. Zou, X. Wang, A. Khan, P. Wang, Y. Liu, A. Alsaedi, T. Hayat and X. Wang, Environmental remediation and application of nanoscale zero-valent iron and its composites for the removal of heavy metal ions: A review, *Environ. Sci. Technol.*, 2016, **50**, 7290-7304.

10. B. Gu, L. Liang, M. J. Dickey, X. Yin and S. Dai, Reductive precipitation of uranium(VI) by zero-valent iron, *Environ. Sci. Technol*., 1998, **32**, 3366-3373.

11. F. Fu, D. D. Dionysiou and H. Liu, The use of zero-valent iron for groundwater remediation and wastewater treatment: A review, *J. Hazard. Mater.*, 2014, **267**, 194-205.

12. J. A. de Lima Perini and R. F. P. Nogueira, Effect of particle size, iron ligands and anions on ciprofloxacin degradation in zero-valent iron process: Application to sewage treatment plant effluent, *J. Chem. Technol. Biotechnol*., 2017, **92**, 2300-2308.

13. A. B. Cundy, L. Hopkinson and R. L. D. Whitby, Use of iron-based technologies in contaminated land and groundwater remediation: A review, *Sci. Total Environ.*, 2008, **400**, 42-51.

14. D. Boglaienko, H. P. Emerson, Y. Katsenovich and T. G. Levitskaia, Comparative analysis of ZVI materials for reductive separation of ^{99}Tc(VII) from aqueous waste streams, *J. Hazard. Mater.,* 2019*,* **380***,* 120836.

15. D. Boglaienko, J. A. Soltis, R. K. Kukkadapu, Y. Du, L. E. Sweet, V. E. Holfeltz, G. B. Hall, E. C. Buck, C. U. Segre, H. P. Emerson, Y. Katsenovich and T. G. Levitskaia, Spontaneous redox continuum reveals sequestered technetium clusters and retarded mineral transformation of iron, *Commun. Chem.,* 2020, **3**(87).

16. M. Jang, B. Park, H. Lee, T.-Y. Kim and Y. Kim, Removal of hexavalent chromium ion from aqueous solution using nanoscale zero-valent iron particles immobilized on porous silica support prepared by polymer template method, *Korean J. Chem. Eng*., 2018, **35**, 2015-2023.

17. D. Shi, G. Zhu, X. Zhang, M. Cheng, T. Wu, K. Zhang and J. Fan, Decorating of ultra small and recyclable nanoscale zero-valent iron on NH_2-SiO_2 for enhanced high-performance removal of water pollutants, *J. Alloy Compd.,* 2019, **782**, 183-192.

18. N. Shukla, V. Gupta, A. S. Rawat, V. K. Gahlot, S. Shrivastava and P. K. Rai, 2, 4-Dinitrotoluene (DNT) and 2, 4, 6-Trinitrotoluene (TNT) removal kinetics and degradation mechanism using zero valent iron-silica nanocomposite, *J. Environ. Chem. Eng.,* 2018, **6**, 5196-5203.

19. S. Chen, J. Bedia, H. Li, L. Y. Ren, F. Naluswata and C. Belver, Nanoscale zero-valent iron@mesoporous hydrated silica core-shell particles with enhanced dispersibility, transportability and degradation of chlorinated aliphatic hydrocarbons, *Chem. Eng. J.,* 2018, **343**, 619-628.

20. L. Honetschlägerová, P. Janouškovcová, M. Velimirovic, M. Kubal and L. Bastiæns, Using silica coated nanoscale zerovalent particles for the reduction of chlorinated ethylenes, *Silicon,* 2018, **10**, 2593-2601.

21. H. Lu, J. Dong, M. Zhang, W. Hu, C. Wen, C. Yang and Y. Wu, SiO_2-coated zero-valent iron nanocomposites for aqueous nitrobenzene reduction in groundwater: Performance, reduction mechanism and the effects of hydrogeochemical constituents, *Colloid. Surface A,* 2018, **558**, 271-279.

22. J. G. Darab, A. B. Amonette, D. S. D. Burke and R. D. Orr, Removal of pertechnetate from simulated nuclear waste streams using supported zerovalent iron, *Chem. Mater*., 2007, **19**, 5703-5713.

23. K. Schwochau, Technetium, Wiley-VCH, 2000.

24. T. A. Marshall, K. Morris, G. T. W. Law, J. F. W. Mosselmans, P. Bots, S. A. Parry and S. Shaw, Incorporation and retention of 99-Tc(IV) in magnetite under high pH conditions, *Environ. Sci. Technol*., 2014, **48**, 11853-11862.

25. S. A. Saslow, W. Um, C. I. Pearce, M. H. Engelhard, M. E. Bowden, W. Lukens, I. I. Leavy, B. J. Riley, D.-S. Kim, M. J. Schweiger and A. A. Kruger, Reduction and simultaneous removal of ^{99}Tc and Cr by $Fe(OH)_2$(s) mineral transformation, *Environ. Sci. Technol*., 2017, **51**, 8635-8642.

26. E. Yalçintaş, A. C. Scheinost, X. Gaona and M. Altmaier, Systematic XAS study on the reduction and uptake of Tc by magnetite and mackinawite. *Dalton Trans*., 2016, **45**, 17874-17885.

27. W. W. Lukens and S. A. Saslow, Facile incorporation of technetium into magnetite, magnesioferrite, and hematite by formation of ferrous nitrate in situ: precursors to iron oxide nuclear waste forms, *Dalton Trans*., 2018, **47**, 10229-10239.

28. W. Um, H.-S. Chang, J. P. Icenhower, W. W. Lukens, R. J. Serne, N. P. Qafoku, J. H. Jr. Westsik, E. C. Buck and S. C. Smith, Immobilization of 99-Technetium (VII) by Fe(II)-Goethite and limited reoxidation, *Environ. Sci. Technol*., 2011, **45**, 4904-4913.

29. N. R. Overman, X. Jiang, R. K. Kukkadapu, T. Clark, T. J. Roosendaal, G. Coffey, J. E. Shield and S. N. Mathaudhu, Physical and electrical properties of melt-spun Fe-Si (3–8 wt.%) soft magnetic ribbons, *Mater. Charact.,* 2018, **136**, 212-220.

30. X. Zhao, W. Liu, Z. Cai, B. Han, T. Qian and D. Zhao, An overview of preparation and applications of stabilized zero-valent iron nanoparticles for soil and groundwater remediation, *Wat. Res*., 2016, **100**, 245-266.

31. J. Zhao, F. E. Huggins, Z. Feng and G. P. Huffman, Ferrihydrite: Surface structure and its effects on phase transformation, *Clay Clay Miner*., 1994, **42**, 737-746.

32. Y. Tamaura, K. Ito and T. Katsura, Transformation of γ-FeO(OH) to Fe_3O_4 by adsorption of iron(II) ion on γ-FeO(OH), *J. Chem. Soc. Dalton Trans*., 1983, **2**, 189-194.

33. P. J. Swedlund and J. G. Webster, Adsorption and polymerization of silicic acid on ferrihydrite, and its effect on arsenic adsorption, *Wat. Res*., 1999, **33**, 3413-3422.

34. R. M. Cornell and U. Schwertmann, The iron oxides: structure, reactions, occurrences and uses, second ed., Wiley-VCH, 2003.

35. I. M. Ali, E. S. Zakaria, M. M. Ibrahim and I. M. El-Naggar, Synthesis, structure, dehydration transformations and ion exchange characteristics of iron-silicate with various Si and Fe contents as mixed oxides, *Polyhedron*, 2008, **27**, 429-439.

36. R. K. Iler and R. Iler, The chemistry of silica: solubility, polymerization, colloid and surface properties, and biochemistry, J. Wiley & Sons, NY, 1979.

37. C. C. Davis, H.-W. Chen and M. Edwards, Modeling silica sorption to iron hydroxide. *Environ. Sci. Technol*., 2002, **36**, 582-587.

38. X. Wang, J. D. Kubicki, J.-F. Boily, G. A. Waychunas, Y. Hu, X. Feng and M. Zhu, Binding geometries of silicate species on ferrihydrite surfaces, *ACS Earth Space Chem*., 2018, **2**, 125-134.

39. A. C. Makrides, M. Turner and J. Slaughter, Condensation of silica from supersaturated silicic acid solutions, *J. Colloid Interf. Sci*., 1980, **73**, 345-367.

40. X. Gao, R. A. Root, J. Farrell, W. Ela and J. Chorover, Effect of silicic acid on arsenate and arsenite retention mechanisms on 6-L ferrihydrite: A spectroscopic and batch adsorption approach, *Appl. Geochem.,* 2013, **38**, 110-120.

41. X. Yang, P. Roonasi, R. Jolsterå and A. Holmgren, Kinetics of silicate sorption on magnetite and maghemite: An in situ ATR-FTIR study, *Colloid. Surface A*, 2009, **343**(1-3), 24-29.

42. T. W. Swaddle and P. Oltmann, Kinetics of the magnetite–maghemite–hematite transformation, with special reference to hydrothermal systems, *Can. J. Chem*., 1980, **58**(17), 1763-1772.

43. C. A. Gorski and M. M. Scherer, Determination of nanoparticulate magnetite stoichiometry by Mössbauer spectroscopy, acidic dissolution, and powder X-ray diffraction: A critical review, *Am. Mineral*., 2010, **95**, 1017-1026.

44. P. Larese-Casanova, A. Kappler and S. B. Haderlein, Heterogeneous oxidation of Fe(II) on iron oxides in aqueous systems: Identification and controls of Fe(III) product formation, *Geochim. Cosmochim. Acta,* 2012, **91**, 171-186.

45. E. Brok, C. Frandsen, D. E. Madsen, H. Jacobsen, J. O. Birk, K. Lefmann, J. Bendix, K. S. Pedersen, C. B. Boothroyd, A. A. Berhe, G. G. Simeoni and S. Mørup, Magnetic properties of ultra-small goethite nanoparticles, *J. Phys. D: Appl. Phys*., 2014, **47**, 365003.

46. G. F. Goya, T. S. Berquó and F. C. Fonseca, Static and dynamic magnetic properties of spherical magnetite nanoparticles, *J. Appl. Phys*., 2003, **94**, 3520-3528.

47. G. M. da Costa, E. De Grave and R. E. Vandenberghe, Mössbauer studies of magnetite and Al-substituted maghemites, *Hyperfine Interact.,* 1998, **117**, 207-243.

48. Y. Masue-Slowey, R. H. Loeppert and S. Fendorf, Alteration of ferrihydrite reductive dissolution and transformation by adsorbed As and structural Al: Implications for As retention, *Geochim. Cosmochim. Acta*, 2011, **75**(3), 870-886.

49. A. G. B. Williams and M. M. Scherer, Spectroscopic evidence for Fe(II)-Fe(III) electron transfer at the iron oxide-water interface, *Environ. Sci. Technol*., 2004, **38**, 4782-4790.

50. T. V. Do, J. M. Joseph, G. Whitaker, B. Noye, V. Bostan, D. Jarron and J. C. Wren, Methodology for Volume Reduction of Radioactive Metallic Waste, WM 2019 Symposia, March 3-7, Phoenix, AZ 2019.

51. P. Hantz, Pattern formation in a new class of precipitation reactions, PhD diss., Université de Genève, 2006.

52. K. H. Stern, The Liesegang Phenomenon, *Chem. Rev.*, 1953, **54**(1), 79-99.

53. D. J. Leveson, Orbicular rocks: A Review, *Geol. Soc. Am. Bull.*, 1966, **77**, 409-426.

54. J. George and G. Varghese, Intermediate colloidal formation and the varying width of periodic precipitation bands in reaction-diffusion systems, *J. Colloid Interf. Sci.*, 2005, **282**, 397-402.

55. I. L'Heureux, Self-organized rhythmic patterns in geochemical systems, *Philos. T. Roy. Soc. A,* 2013, **371**(2004), 20120356.

56. H. Meinhardt, The algorithmic beauty of sea shells, Springer, 4th ed., 2009.

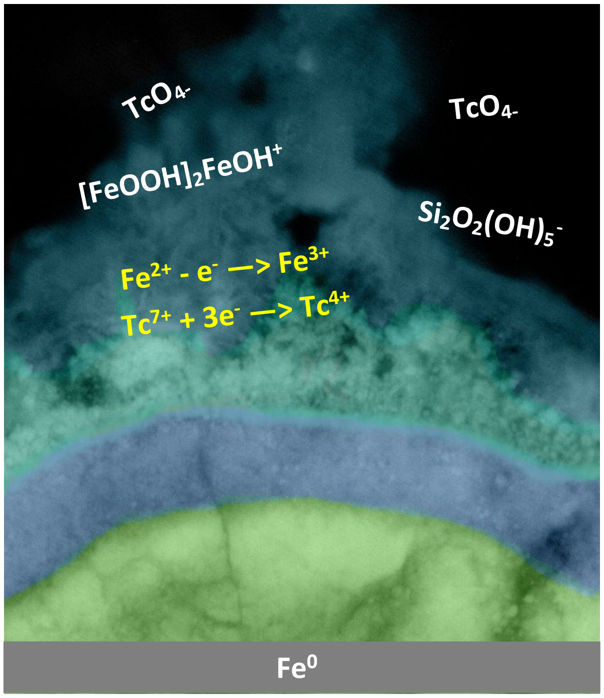

Efficiency of TcO_4^- reduction by metallic Fe^0 increases in the presence of silica due to inhibited transformation of iron oxyhydroxide to non-stoichiometric magnetite. Rhythmical dissolution/re-precipitation of dissolved iron leads to formation of layered structures related to such geological phenomena as Orbicular rocks and Liesegang rings.